Particle Sedimentation during Processing of Liquid Metal-Matrix Composites

G.S. HANUMANTH, G.A. IRONS, and S. LAFRENIERE

A novel electrical resistance probe technique to measure the *in situ* volume fraction of ceramic particles in molten metals was applied to the measurement of sedimentation rates of 90-μm-diameter silicon carbide particles in molten aluminum. The results indicate that the rate strongly depends on volume fraction; the time to clarify a 0.15-m depth increased from approximately 60 to 500 seconds as the particle volume fraction increased from 0.05 to 0.30. Maps showing the changes in volume fraction throughout the melt were generated. A multiphase hydrodynamic model was developed to describe the sedimentation. Using volume fraction-dependent drag coefficients from work in aqueous systems, the model was able to simulate the experimental results remarkably well. The experimental and modeling results indicate that there was little agglomeration or network formation during sedimentation. The implications of the results for solidification and particle pushing are discussed.

I. INTRODUCTION

METAL-matrix composites (MMCs) are a relatively new class of engineering materials in which a strong ceramic phase is added to a metal matrix. Most work has been performed on the addition of SiC and Al_2O_3 fibers and particles to aluminum alloys.[1] While there has been considerable amount of research on the mechanical properties of such materials, there has been comparatively little research on the fundamentals of MMC processing.

There are four major processing routes to make MMCs:

(1) blending of metal and ceramic powders by powder metallurgy techniques;
(2) infiltration of liquid metal into preforms of ceramic fibers or particles;
(3) spray deposition of streams of molten metal and ceramic particles onto a substrate; and
(4) stirring of ceramic particles into melts.

The fourth method is potentially the cheapest in situations where only moderate improvements over the unreinforced alloy are required. ALCAN has commercialized a process based on this technique in which SiC or Al_2O_3 is stirred into molten aluminum.[1]

In the particle mixing techniques, there are three major fundamental problems:

(1) most particles are not easily wetted;[2]
(2) the particles either sink or float in the melt, depending on the ratio of particle-to-liquid density; and
(3) the viscosities of the mixtures are very high and are also time- and shear rate-dependent.[3]

In an aluminum-silicon carbide particle composite, the silicon carbide particles tend to settle because they are denser than the melt (ρ_{Al} = 2400 kg/m^3, ρ_{SiC} = 3200 kg/m^3). Typically, the particles are stirred into the melt with a mechanical stirrer. Following mixing, the molten mixture must be transferred to the mold. Consequently, there can be some time between the end of stirring and complete solidification. Obviously, to obtain a homogeneous composite, solidification must occur before appreciable settling has taken place. Very little work has been performed on sedimentation of particles in liquid metals, despite the industrial importance of the subject.

In the present work, a novel probe to measure the *in situ* volume fraction of the particles was developed. Using this probe, it was possible to observe the changes of volume fraction with time. The experimental results were interpreted within the framework of a mathematical model developed from multiphase hydrodynamic flow theory to provide a quantitative understanding of the phenomena.

II. LITERATURE REVIEW

To the authors' knowledge, there has never been a systematic study of particle sedimentation in liquid metals, particularly at high volume fractions characteristic of MMCs, namely, up to 0.30 volume fraction. The high temperatures and opacity of the melt have precluded simple techniques for observation of sedimentation that have been utilized in aqueous systems. However, it is instructive to review the extensive literature of sedimentation in aqueous systems.

For a single particle settling in an infinite expanse of liquid, the sedimentation rate can be calculated using the well-known Stokes law:[4]

$$U_0 = \frac{g d_p^2 (\rho_p - \rho_L)}{18 \mu_L} \quad [1]$$

As the particle concentration increases beyond the dilute range, the settling of a particle will be influenced by the presence of other particles in the suspension, leading to what is commonly called hindered settling. Because of its enormous practical importance in the chemical and metallurgical process industry, hindered settling in aqueous systems has been the subject of numerous investigations.

G.S. HANUMANTH, Research Associate, and G.A. IRONS, Professor and Chairman, are with the Department of Materials Science and Engineering, McMaster University, Hamilton, ON L8S 4L7, Canada. S. LAFRENIERE, formerly Graduate Student, McMaster University, is Graduate Student, Department of Mining and Metallurgy, Laval University, PQ, Canada.

Manuscript submitted February 21, 1992.

Typical settling behavior is illustrated in Figure 1, which shows the evolution of a liquid-particle suspension due to sedimentation. Initially, the column contains a uniform suspension, B. A clarified liquid region, A, appears when particle sedimentation commences. The settling interface forms a moving boundary between region A and the adjacent region B, where the particle concentration is equal to the initial volume fraction. A dense sediment D, with particle concentration equal to the final volume fraction, builds up at the bottom of the column. In addition, an intermediate region of variable concentration, C, may be present in the column. Regions B and C eventually disappear, as they are compressed into D.

One of the earliest studies was that of Kynch,[5] who postulated that the sedimentation velocity, U_s, was a unique function of the solid volume fraction, θ_s, and derived an expression to calculate the solid flux as a function of θ_s, based on the mass balance equation and knowledge of the movement of the settling interface. Tiller[6] considered the influence of the rising sediment, which Kynch had neglected, by dividing the sinking suspension into a "sedimenting zone" and a compressible sediment zone. The "sedimenting zone" was described by a Kynch-type continuity equation. In the compressible sediment zone, an additional equation of Darcy type for liquid flow was coupled to the continuity equation. A graphical interpretation of the equations was carried out using experimental sedimentation data.

Perhaps the most useful approach was the empirical study of Richardson and Zaki.[7] They showed by an elegant dimensional analysis that, for the settling of nonflocculating, monodisperse, spherical particles, the ratio, U_s/U_0, is a function of the void fraction, resulting in what is now known as the Richardson-Zaki equation:

$$U_s = U_0(1 - \theta_s)^n \quad [2]$$

The value of the exponent n depends on the Reynolds number; in the creeping flow regime, values of n between 4.6 and 5 have been reported by various authors.

Wallis[8] developed a graphical technique to predict sedimentation behavior of a suspension based on experimental measurement of the velocity of continuity waves and shocks. Lafreniere and Irons[9] employed this approach to characterize the settling behavior of SiC particles in molten aluminum alloys.

Generally, the above approaches have not incorporated fundamental information regarding the forces acting between the phases and are based on system-specific experimental data. To develop a more fundamental approach, momentum equations, containing information on drag, must be formulated and solved. One of the most useful approaches to describe the dynamics of particle sedimentation is based on the application of mass and momentum balance equations separately for the fluid and particulate phases. This multiphase approach has been used previously by Dixon[10] and Tiller.[6] Recently, Shih *et al.*[11] developed a one-dimensional hydrodynamic model for the sedimentation of multisized particles. Their model was numerically tedious and required the use of a supercomputer to solve it.

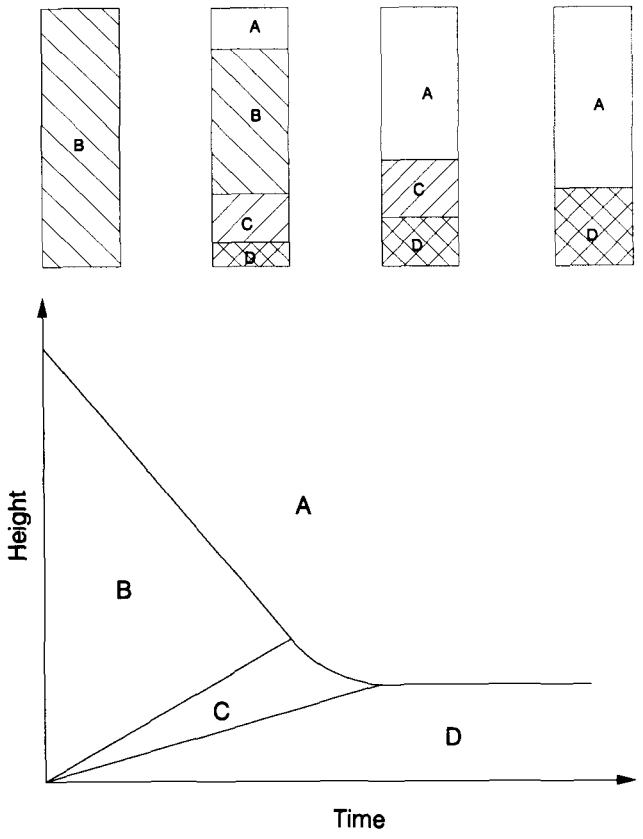

Fig. 1—(Upper) Evolution of a liquid-particle suspension due to sedimentation from the original density B to a clarified region A, and a region of maximum final density D, after passing through an intermediate region C. (Lower) The position of the fronts between regions as a function of time according to upper portion of this figure.

III. EXPERIMENTAL

A. *Apparatus*

The sedimentation experiments were carried out in an alumina crucible of 0.30-m inside diameter and 0.46-m height which was placed inside a resistance-heated furnace (Figure 2). The melt surface was exposed to air. The SiC particles were mixed into the melt with a pitched-blade turbine impeller, fabricated from graphite, and driven by a variable speed AC motor. The impeller shaft was made of mild steel and enclosed in a graphite sleeve to avoid contact with the aluminum. All joints were sealed with a high-temperature ceramic adhesive.

The resistivity measurements were taken automatically with a commercially available micro-ohmmeter (TECRAD DMO 350). The DMO 350 is a portable, microprocessor-controlled, high accuracy micro-ohmmeter which was designed for the measurement of the electrical resistance of solid, room-temperature alloys. The micro-ohmmeter was connected to a computer through an RS232 port. The computer controlled the micro-ohmmeter, stored the measurements, and performed data reduction.

For use in liquid aluminum, a four-point resistivity probe was developed (Figure 3). It was constructed from stainless steel and coated with an alumina paste. The two

outer electrodes were used to carry a brief (30 ms) DC electrical pulse. The microresistance across the inner two electrodes was measured simultaneously. The electrodes were made of tungsten soldered to silver wires. The tungsten and silver wires were 1.4 and 1.0 mm in diameter, respectively. Tungsten was chosen because of its resistance to dissolution in liquid aluminum, and silver because of its resistance to oxidation at high temperature.

The particle size distribution of the green silicon carbide particles used in the experiments (supplied by Norton Advanced Ceramics of Canada, Niagara Falls, Canada) was measured with a Horiba CAPA-700 particle analyzer (Horiba Ltd., Kyoto, Japan). The mean Stokes equivalent diameter was found to be 90 μm, with a standard deviation of 19 μm. A commercial foundry alloy, A356 (supplied by ALCAN), which is often used for MMCs, was used. The major alloying elements are 7.3 pct Si and 0.33 pct Mg.

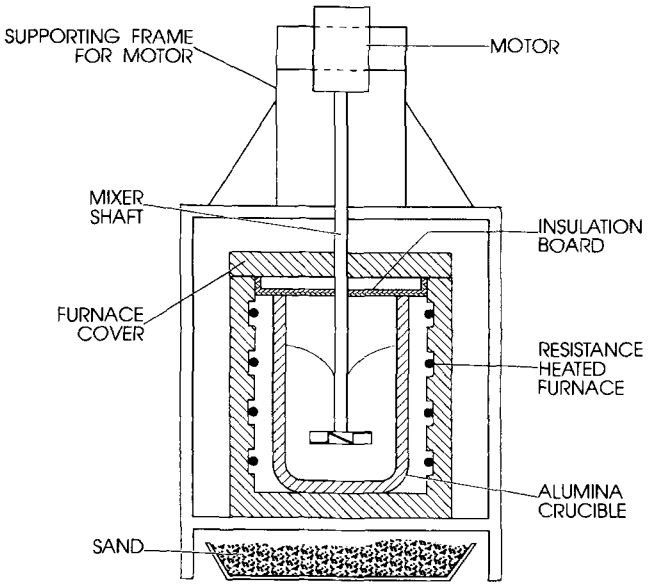

Fig. 2—Schematic diagram of the experimental apparatus.

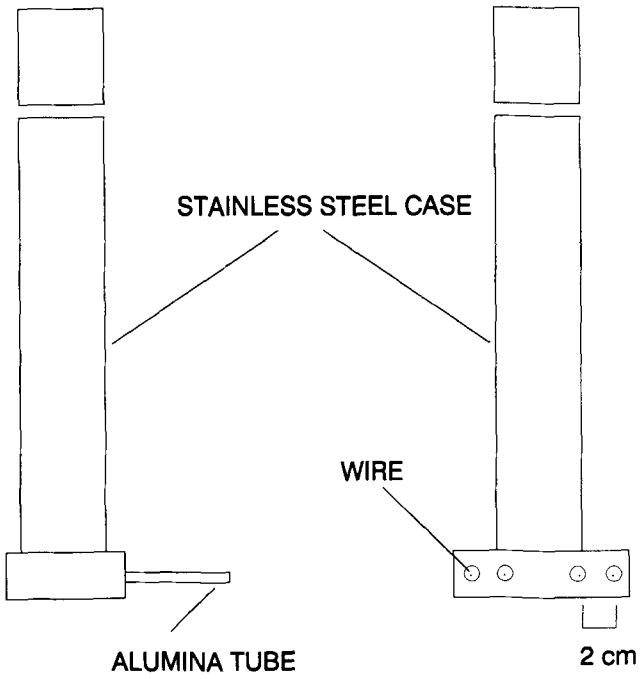

Fig. 3—Schematic diagram of the four-point probe. The two outer electrodes carry the applied current, while the inner two are used for resistance measurement.

B. *Procedure*

Initially 27.2 kg of the alloy was charged to the crucible to produce a melt depth of 210 mm. The melt was maintained at 660 °C. The probe was then lowered into the melt beside the stirrer and fixed at a depth of 50 mm from the melt surface. Subsequently, 0.05 volume fraction SiC particles were added to the melt and mixed at a speed of 525 rpm for 10 minutes. At the end of the mixing time, the mixer was stopped and resistance measurement was started at the same instant. The resistance was measured every two seconds, until the settling interface had passed the probe. The measurement procedure was repeated three times to ensure reproducibility of the results.

The above procedure was carried out for three different probe locations: 50, 100, and 150 mm below the melt surface. The SiC volume fraction was increased in steps of 0.05 to a final concentration of 0.3.

C. *Results*

Figure 4 shows the increase in resistance of the A356 alloy due to SiC particle addition, plotted as a function of the particle volume fraction. The resistance increases linearly with volume fraction in the volume fraction range of 0 to 0.3. The closeness of the curves at different depths of immersion of the probe indicates that the particles are sufficiently well dispersed in the melt under the mixing conditions mentioned in the experimental procedure. An

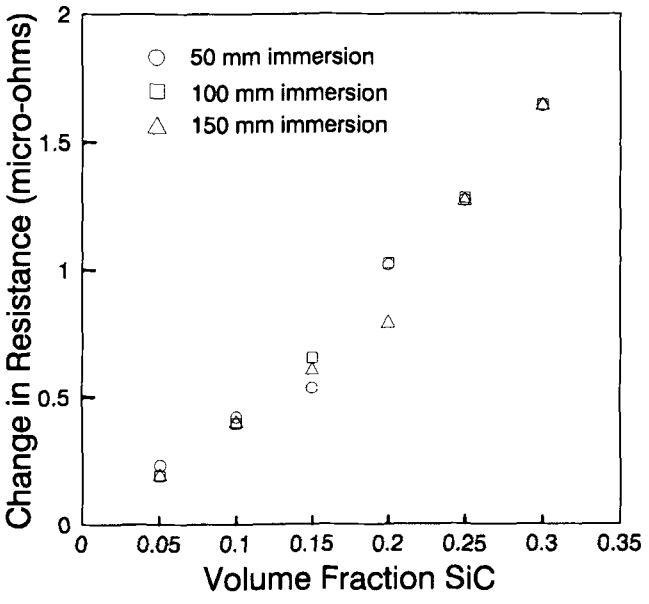

Fig. 4—Change in resistance measured by the probe during sedimentation for different initial particle volume fractions.

independent confirmation of the homogeneity of the composite was obtained by the microscopic examination of a rapidly solidified pin sample, withdrawn by suction into a narrow PYREX* tube from near the center of the bulk composite. The microstructure of such a sample for the 0.3 volume fraction composite is shown in Figure 5. The nonagglomerated homogeneous distribution of the particles in the composite is apparent in this sample.

*PYREX is a trademark of Corning Glass Works, Corning, NY.

With the onset of sedimentation, the resistance of the melt decreases due to particle settling. The output of the probe during sedimentation as a function of time for three different immersion depths is shown in Figures 6 and 7 for initial volume fractions of 0.1 and 0.3, respectively.

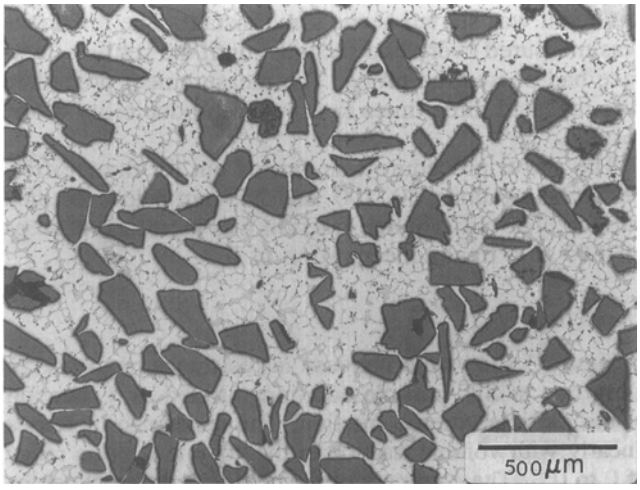

Fig. 5—Microstructure of the cross section of an A356-SiC composite, with a particle volume fraction of 0.3.

In each case, the resistance drops as the settling interface passes the probe location. The time for the transition takes longer for deeper immersions. For the 150-mm immersion in the 0.3 volume fraction case, the readings increase because the probe becomes surrounded by denser sediment. This does not occur at lower volume fractions, as the sediment is not sufficiently deep to reach the probe level. The time for the clarification front to pass the probe was approximately 60 seconds in Figure 6 for the 0.1 volume fraction case; however, this time increased to about 500 seconds for the 0.3 volume fraction case.

Diagrams such as Figure 1 can be deduced from the time-resistance curves because the drop in resistance is due to clarification of the melt. The time taken to attain a lower value is therefore a measure of the time taken by the settling front to traverse the distance between the melt surface and the probe. For volume fractions greater than 0.1, the resistance curve has a protracted decline, as shown for 0.3 volume fraction in Figure 7, which implies that, at high volume fractions, there is a broadening of settling rate. This broadening of settling rate delays the passage of the clarification front past the probe. This phenomenon is illustrated in the settling curves, for example Figure 10, by constructing bands; the ends of the bands mark the times required for 50 pct change in volume fraction and for complete settling, respectively.

IV. MATHEMATICAL MODEL

The aim of this model is to simulate the sedimentation behavior of high volume fractions of particles settling in liquid aluminum observed in the present work. The following simplifying assumptions are made:

(1) The flow is entirely in the vertical direction, since gravity is the primary force on the system;
(2) The diameter of the container is much larger than

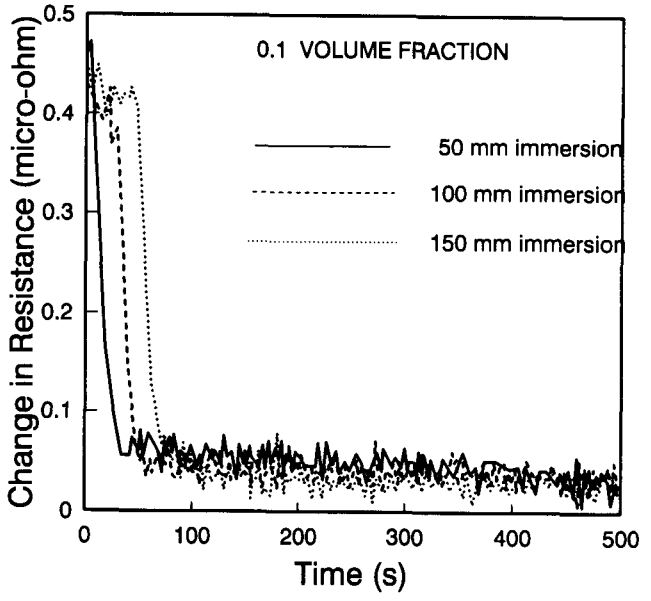

Fig. 6—Change in resistance of the molten composite due to particle sedimentation as a function of time for an initial particle volume fraction of 0.1 and 3 probe immersion depths.

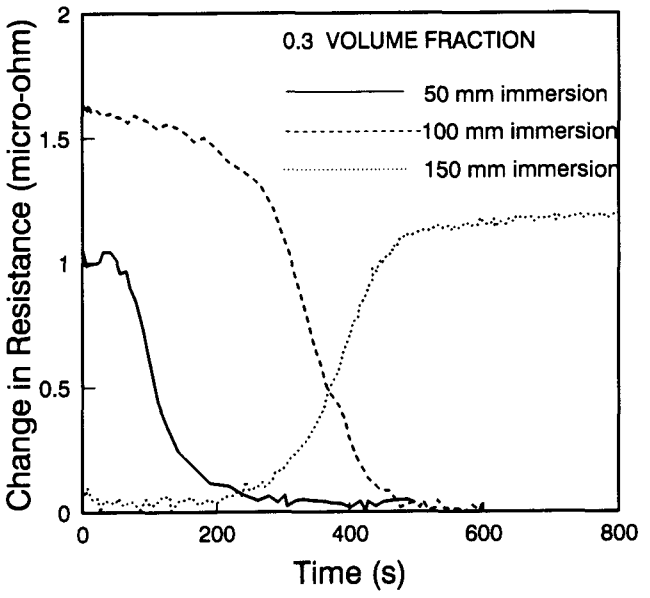

Fig. 7—Change in resistance of the molten composite due to particle sedimentation as a function of time for an initial particle volume fraction of 0.3 and 3 probe immersion depths.

the particle diameter; consequently, wall effects are ignored.
(3) Surface tension and interparticle forces are considered negligible. For sufficiently large particles, the relative magnitude of surface and interparticle forces will be negligible compared to the gravity body forces.
(4) Compressive stresses are neglected. While compressive stresses can be safely neglected in the suspension where particles are unlikely to be in contact, it is somewhat unrealistic to neglect them in the dense sediment layer at the bottom where particles are in contact and the weight of solids above compresses the layer. However, in the absence of any constitutive relationship for compressive stresses in Al/SiC suspensions, it is assumed that when the particle volume fraction reaches 0.6, further compression ceases.
(5) Added mass and history terms are neglected because the acceleration terms are generally small.

Equations for unsteady-state conservation of mass and momentum are written for each phase, using multiphase flow theory:[12]

Conservation of Mass

$$\frac{\partial \theta_s}{\partial t} + \frac{\partial (U_s \theta_s)}{\partial x} = 0 \quad \text{(Solids)} \qquad [3]$$

$$\frac{\partial \theta_L}{\partial t} + \frac{\partial (U_L \theta_L)}{\partial x} = 0 \quad \text{(Liquid)} \qquad [4]$$

Conservation of Momentum

$$\rho_s \frac{\partial (U_s \theta_s)}{\partial t} + \rho_s \frac{\partial (U_s^2 \theta_s)}{\partial x} + \theta_s \frac{\partial P}{\partial x} - \rho_s \theta_s g + F_D = 0$$

(Solids) [5]

$$\rho_L \frac{\partial (U_L \theta_L)}{\partial t} + \rho_L \frac{\partial (U_L^2 \theta_L)}{\partial x} + \theta_L \frac{\partial P}{\partial x} - \rho_L \theta_L g - F_D = 0$$

(Liquid) [6]

Since the solid and liquid phases are incompressible, the total volume is invariant; hence, the solids settling velocity, U_s, and the upward liquid velocity, U_L, are not independent but related through a volumetric flux balance expression:

$$U_L = -\frac{U_s \theta_s}{(1 - \theta_s)} \qquad [7]$$

Further, the volumetric fractions must satisfy the overall continuity equation:

$$\theta_s + \theta_L = 1 \qquad [8]$$

The total static pressure gradient can be determined by summing Eqs. [5] and [6] and neglecting acceleration and inertial terms, yielding

$$\frac{\partial P}{\partial x} - (\rho_s \theta_s + \rho_L \theta_L) g = 0 \qquad [9]$$

The bracketed term is the mixture density; thus,

$$\frac{\partial P}{\partial x} = \rho_m g \qquad [10]$$

that is, the pressure drop is simply the weight of the suspension.

Some further manipulation is required to solve the equations for θ_s and U_s. Equation [5] can be simplified by expanding the derivatives using the chain rule and applying the mass balance of Eq. [3]. The result is

$$\frac{\partial U_s}{\partial t} = -U_s \frac{\partial U_s}{\partial x} - \left(\frac{1}{\rho_s}\right) \frac{\partial P}{\partial x} + g - \frac{F_D}{(\rho_s \theta_s)} \qquad [11]$$

Substituting for dp/dx from Eq. [10] yields

$$\frac{\partial U_s}{\partial t} = -U_s \frac{\partial U_s}{\partial x} + \left(1 - \left(\frac{\rho_m}{\rho_s}\right)\right) g - \frac{F_D}{(\rho_s \theta_s)} \qquad [12]$$

The main difficulty in modeling is the proper representation of F_D. The drag force F_D may be a function of the relative velocity $(U_s - U_L)$, viscosity, and volume fraction. A constitutive equation for F_D is derived using a method similar to that of Gidaspow,[13] in which F_D was expressed as

$$F_D = \beta (U_s - U_L) \qquad [13]$$

where β is the friction coefficient given by the expression

$$\beta = \frac{3}{4} C_D \rho_L \theta_L \theta_s \frac{(U_s - U_L)}{d_p} f(\theta_L) \qquad [14]$$

The form of Eq. [14] was chosen to mirror that for single particles. For single particles, β is independent of θ_L; thus, $f(\theta_L)$ is 1. All of the deviations from single particle behavior will be assumed to be captured in the f function.

For the 90-μm SiC particles used in the present work, the Stokes settling velocity (Eq. [1]) is 1.77 mm/s, based upon an aluminum viscosity of 2×10^{-3} kg/m/s. The particle Reynolds number based on Stokes velocity

$$\mathrm{Re}_p = \frac{d_p (U_s - U_L) \rho_L \theta_L}{\mu_L} \qquad [15]$$

is 0.19 and will be smaller under hindered settling conditions. Settling then occurs in the creeping flow regime for which

$$C_D = \frac{24}{\mathrm{Re}_p} \qquad [16]$$

Inserting Eqs. [15] and [16] into Eq. [14], one obtains

$$\beta = \frac{18 \mu_L \theta_s}{d_p^2} f(\theta_L) \qquad [17]$$

The void fraction function $f(\theta_L)$ still needs to be explicitly defined to solve the constitutive equations. This

can be done by neglecting the acceleration and inertial terms in Eq. [12], yielding

$$\left(1 - \left(\frac{\rho_m}{\rho_s}\right)\right) g = \frac{F_D}{(\rho_s \theta_s)} = \frac{\beta(U_s - U_L)}{(\rho_s \theta_s)} \qquad [18]$$

from which β is expressed explicitly as

$$\beta = g\theta_s \frac{(\rho_s - \rho_m)}{(U_s - U_L)} \qquad [19]$$

There are two independent methods to calculate β from Eq. [19]. The first method is based on the Richardson-Zaki equation, while the second method utilizes measured settling velocities. The first method will be developed here, leaving the second for Section V.

The first method utilizes the Richardson-Zaki correlation (Eq. [2]), with the exponent n equal to 4.65,[7] to calculate U_s. Combining this expression with Stokes velocity (Eq. [1]) and a flux balance (Eq. [7]), one obtains, after some manipulation:

$$\beta = \frac{18\mu_L \theta_s}{d_p^2} (1 - \theta_s)^{-2.65} \qquad [20]$$

Comparing Eq. [20] with [17], it is apparent that

$$f(\theta_L) = (1 - \theta_s)^{-2.65} \qquad [21]$$

Hence,

$$F_D = \frac{18\mu_L \theta_s (1 - \theta_s)^{-2.65} (U_s - U_L)}{d_p^2} \qquad [22]$$

Eliminating U_L from Eq. [22] by means of Eq. [7], the momentum equation for the solid phase (Eq. [5]) can be recast in its final form:

$$\frac{\partial U_s}{\partial t} = -U_s \frac{\partial U_s}{\partial x} + \left(1 - \frac{\rho_m}{\rho_s}\right) g - \frac{18\mu_L (1 - \theta_s)^{-3.65} U_s}{\rho_s d_p^2} \qquad [23]$$

Equations [3] and [23] must be solved simultaneously to yield θ_s and U_s as a function of time and position. The liquid velocity and phase fraction can then be obtained from Eqs. [7] and [8]. The sensitivity of the friction coefficient β, given by Eq. [20], to the value of the Richardson-Zaki exponent n was assessed over a range of n values equal to 4.65 ± 10 pct. The resulting variation in the value of β was found to lie between ±2 and ±10 pct as the volume fraction increased from 0.05 to 0.2; positive deviations were associated with higher n values, and negative deviations were associated with lower n values.

A. *Numerical Solution*

The partial differential equations were solved numerically within the settling domain by transforming them into a system of ordinary differential equations by the so-called method of lines.[14] This method essentially consists of discretization of the spatial variable in the time-dependent partial differential equation, with the result that a semidiscrete approximate system of ordinary differential equations are generated. These ordinary differential equations were solved by the well-tested integrator package, called LSODE, developed at the Lawrence Livermore National Laboratory, Livermore, CA.[15]

The solution of the equations is complicated by the presence of the two moving boundaries, specifically, the settling interface, and the rising sediment interface. The nodes at the interfaces were handled separately from the intervening nodes. It was assumed that the suspension is initially uniform and motionless. The suspension in the top layer was allowed to settle with a sharp interface at a velocity given by the Richardson-Zaki equation. At each time step δt, typically 10 ms, the solid volume fraction was updated by

$$\theta_s(1, t + \delta t) = \theta_s(1, t) \left(1 - \frac{U_s(1, t)\delta t}{\delta x}\right) \qquad [24]$$

Similarly, the bottom layer was updated using

$$\theta_s(n, t + \delta t) = \theta_s(n, t) + \left(\frac{U_s(n - 1, t)\delta t}{\delta x}\right) \theta_s(n - 1, t) \qquad [25]$$

With the above boundary conditions, the governing equations (Eqs. [3] and [23]) were solved for intervening nodes with uniform node size and centered difference approximations. The computation proceeded until one of the following conditions was achieved:

(1) The top layer became devoid of particles; *i.e.*, θ_s became less than a predetermined limit, taken as 0.001.
(2) The bottom layer became closely packed with particles; *i.e.*, θ_s became greater than 0.6.
(3) The top layer became devoid of particles and the bottom layer became close-packed simultaneously.

The occurrence of one of the above conditions causes shrinkage of the settling domain by either one or two layers, depending on which of the three conditions occurred. The domain and the spatial mesh were accordingly redefined and new boundary conditions specified corresponding to the end conditions of the last computation. The equations discretized within the new domain were solved as previously described until the procedure once again encountered one of the above conditions. This pattern of computation was repeated until the settling interface and the rising interface converged. At this time, sedimentation was deemed to be complete.

Several mesh sizes ranging from 600 to 100 μm were tested. Since the results were unaffected by halving the mesh size down from 200 to 100 μm, it was decided to select the 200 μm to keep the mesh size substantially greater than the particle size, 90 μm. The time step used in the LSODE code was selected internally; it lay in the range of 0.01 to 100 μs.

B. *Computed Results*

The results of the model are presented graphically in Figures 8 through 12, along with the experimental results. It is apparent that there is reasonably good agreement between experimental and computed results, considering the extrapolation from behavior in aqueous

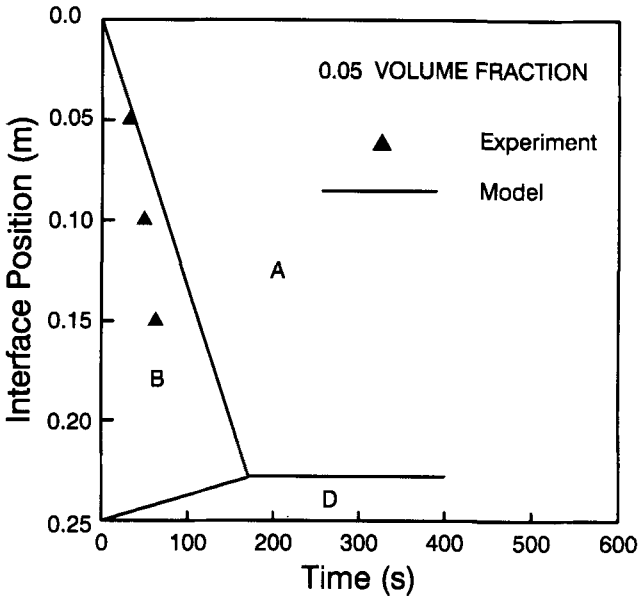

Fig. 8—Position of the clarification front and the rising sediment interface as a function of time during sedimentation of the 0.05 volume fraction composite.

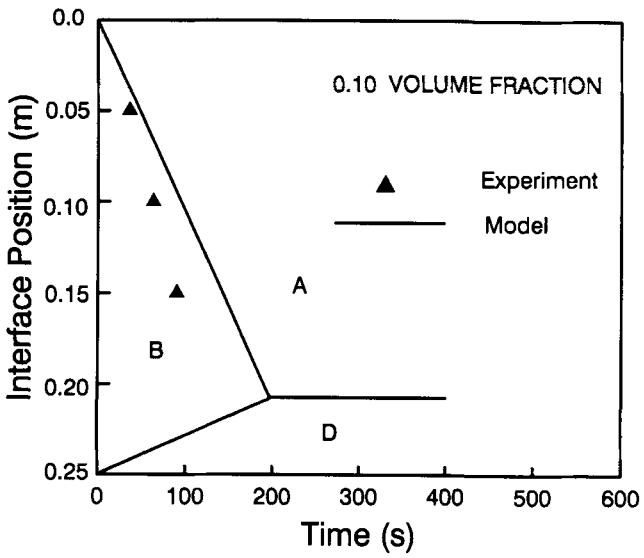

Fig. 9—Position of the clarification front and the rising sediment interface as a function of time during sedimentation of the 0.1 volume fraction composite.

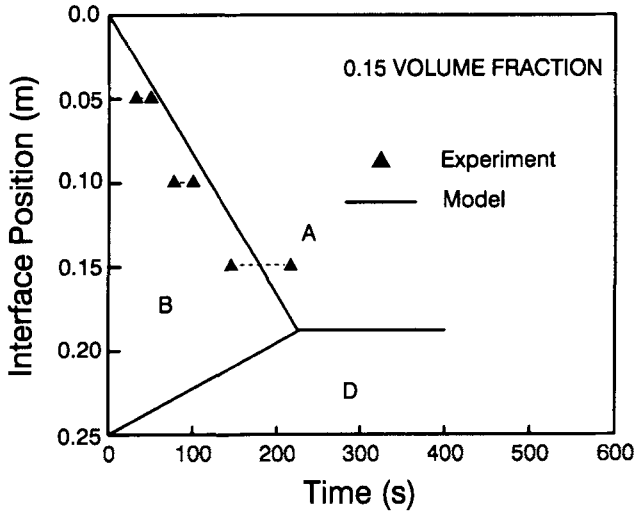

Fig. 10—Position of the clarification front and the rising sediment interface as a function of time during sedimentation of the 0.15 volume fraction composite.

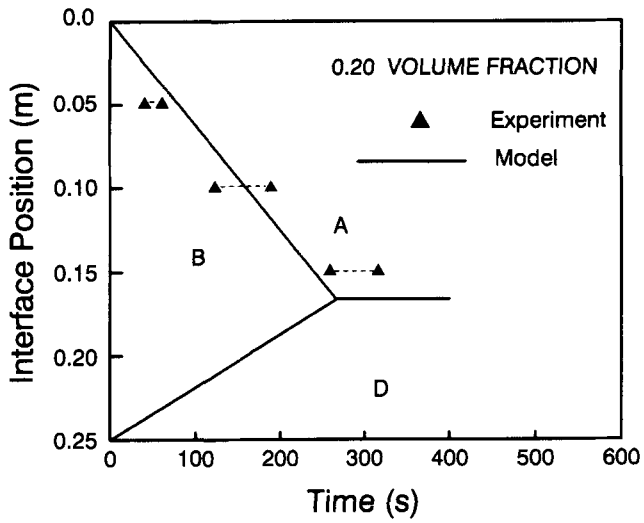

Fig. 11—Position of the clarification front and the rising sediment interface as a function of time during sedimentation of the 0.20 volume fraction composite.

systems. Looking more closely, one observes that the model predicts lower settling velocities at 0.05 and 0.1 volume fraction as compared to the experiments. At the higher volume fractions, 0.15, 0.20, and 0.30, there is better agreement in the settling velocities. At a volume fraction of 0.3, the rate of rise of the sediment-suspension interface can be measured because the sediment grows to sufficient thickness to cover the probe when it is located at an immersion of 150 mm. For this case, the computed rate of sediment-suspension interface rise is observed to agree well with the experimental value.

The settling curves for the model are essentially linear, while for the shallowest immersion, the experimental curves for volume fractions 0.05 and 0.10 may exhibit a change of slope. This may be due to the persistence of motion of the suspension after mechanical mixing was stopped. This phenomenon may not have been visible at high volume fractions because of the damping effect of high suspension viscosity.

As the particle volume fraction increases from 0.05 to 0.3, the settling rate decreases. A further effect of increased volume fraction appears to be that, as volume fraction increases to 0.15 and 0.30, the settling rate becomes time-dependent, decreasing as time progresses in the experiment. The predicted settling rates are much lower in magnitude at volume fractions 0.05 and 0.10 than measured values but tend to approach experimental values at 0.15 to 0.30.

V. DISCUSSION

The predicted settling curves are all practically linear, suggesting that the inertial and acceleration terms in

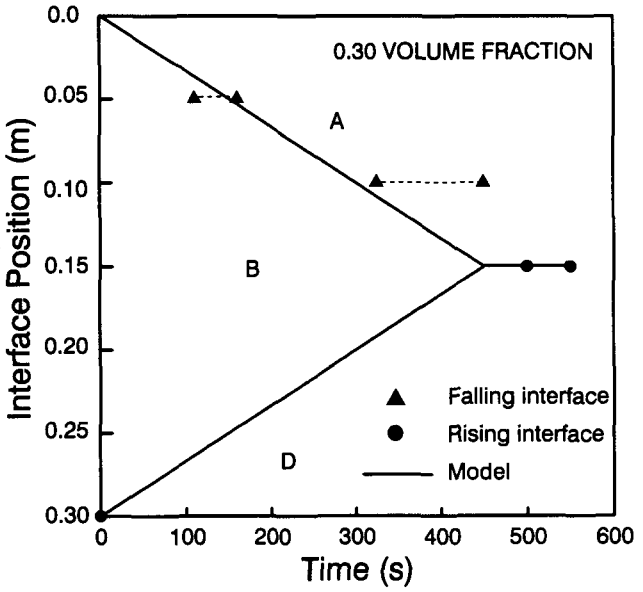

Fig. 12—Position of the clarification front and the rising sediment interface as a function of time during sedimentation of the 0.30 volume fraction composite.

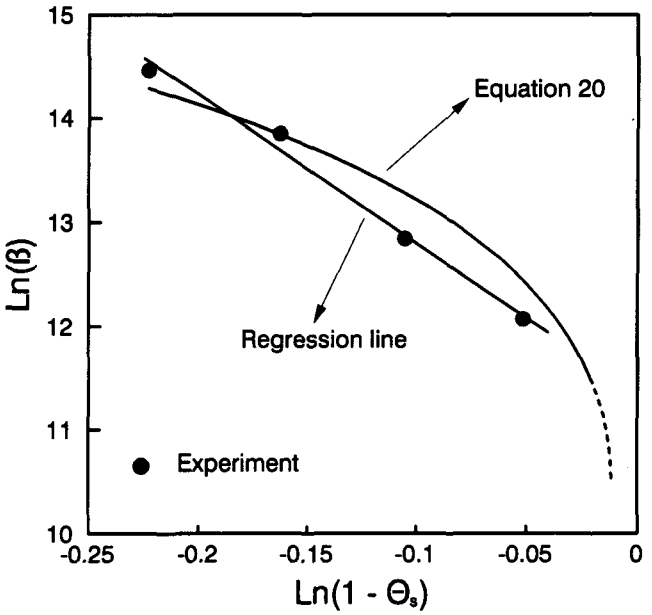

Fig. 13—The power-law function (Eq. [26]) fitted to experimental values of the friction coefficient β. The power-law coefficients are $\beta_0 = 8.8 \times 10^4$ and $m = -14$.

Eqs. [5] and [6] are rather small. This finding justifies assumption 5, in which the added mass and history terms were ignored. Furthermore, the particles will settle at a rate determined essentially by a balance between buoyancy and drag force, which are functions of particle volume fraction and time.

While there is good agreement between the model and experiments, the lower settling rates predicted by the model at volume fractions 0.05 and 0.10, in comparison to the experiments, indicate that the model has a somewhat stronger dependence on the volume fraction at concentrations of up to 0.10 than can be accounted for with a drag term arising from the Richardson-Zaki equation. As mentioned earlier, the second method to determine the drag term is to match it to experimental data.

In the second method, it is postulated that the friction coefficient β in Eq. [13] is a power-law function of volume fraction:

$$\beta = \beta_0(1 - \theta_s)^m \qquad [26]$$

wherein β_0 and m are determined empirically. This was done by calculating velocities at different volume fractions, given by the slope of the experimental settling curves. With these velocities, β was estimated as a function of volume fraction, using Eq. [19]. Then the power-law coefficients were obtained by fitting Eq. [26] to these experimental points on logarithmic scales (Figure 13). The resulting function was

$$\beta = 8.8 \times 10^4(1 - \theta_s)^{-14} \qquad [27]$$

Inserting this expression for β into Eq. [13] yields a new empirical equation for the drag force. With this new expression for the drag force, the model provides better agreement with experiment at volume fractions 0.05 and 0.10, as shown in Figures 14 and 15, compared to Figures 8 and 9.

It may be reasoned that the particle size distribution

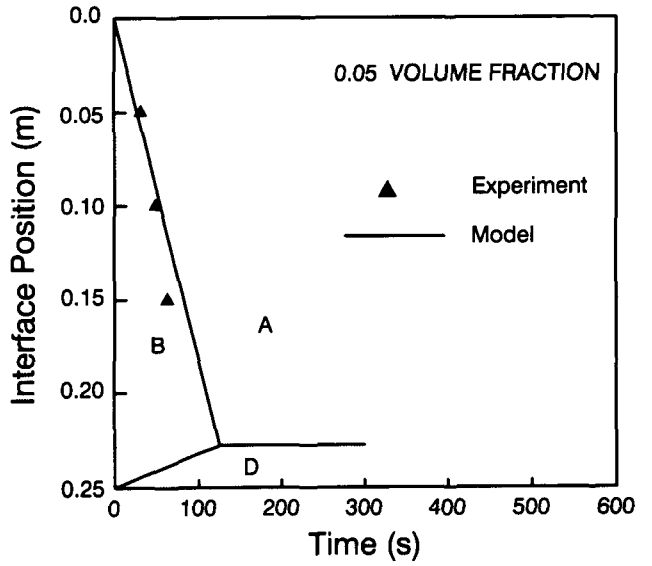

Fig. 14—Position of the clarification front and the rising sediment interface as a function of time during sedimentation of the 0.05 volume fraction composite. Predicted results were obtained by using Eq. [27] for the friction coefficient β.

may be responsible for the broadening of the settling rate curves at higher volume fractions. The present model was extended to a bi-disperse mixture composed of equal volumes of 71- and 90-μm particles; 71 μm was chosen because the standard deviation for the experimental powder was 19 μm from the mean size of 90 μm. In the model, another equation is written for the 71-μm particles, and the continuity equation is modified to include both particle sizes. The results are plotted in Figures 16 and 17. Comparing the difference in rates for the two particle sizes, it is apparent that there is less difference

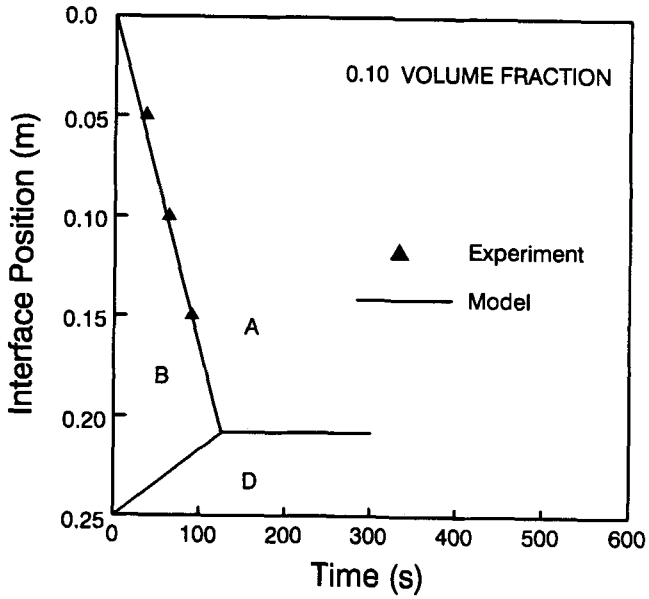

Fig. 15—Position of the clarification front and the rising sediment interface as a function of time during sedimentation of the 0.10 volume fraction composite. Predicted results were obtained by using Eq. [27] for the friction coefficient β.

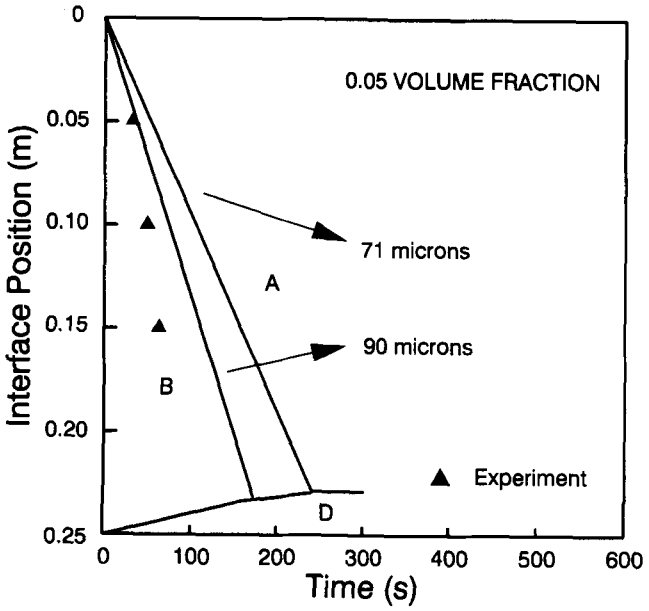

Fig. 16—Sedimentation behavior of a 50/50 bidisperse composite, consisting of 71- and 90-μm SiC particles making up an initial total volume fraction of 0.05. The experimental data of Fig. 8 have been superimposed for the purpose of comparison.

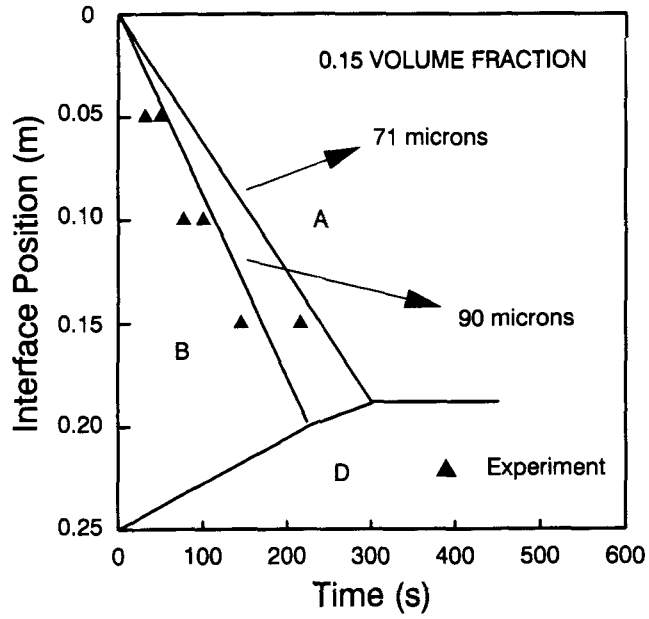

Fig. 17—Sedimentation behavior of a 50/50 bidisperse composite, consisting of 71- and 90-μm SiC particles making up an initial total volume fraction of 0.15. The experimental data of Fig. 10 have been superimposed for the purpose of comparison.

at higher volume fraction; that is, there is less broadening at higher volume fractions, which is opposite to the effect observed in the experimental work. The model behaves this way because, as the volume fraction increases, the settling velocities of all particles should decrease to zero. Therefore, the broad size distribution of particles cannot explain the broad range of settling velocities at high volume fractions.

The present approach to modeling is quite useful because it permits particles of various density or size to be treated simultaneously. Momentum equations may be written for as many categories of particles as required. The momentum equations, along with the one for the liquid, are solved simultaneously, subject to the total solid continuity equation. Thus, broad particle size distributions or mixtures of two types of particles may be modeled.

For the 90-μm particles in this study, it was found that the drag coefficient extracted from the Richardson-Zaki equation provided a surprisingly good estimate for the settling rate, considering that this represents an extrapolation from aqueous systems. The success of the Richardson-Zaki equation also implies that the particles do not significantly cluster or form networks during settling. Further evidence that clustering is unlikely can be found in Figure 12. At the deepest probe location, the rising sediment engulfs the probe. The probe reading corresponds to a volume fraction of 0.6, characteristic of random close packing. Clustering or network formation would not permit such high densities to be achieved. There may be a slight tendency for clustering at high volume fraction, where the clarification front appears to slow down at longer times, as seen in Figures 9 and 10. However, due to the broadening of the front at these times, it is not possible to positively identify clustering phenomena.

Particles used in commercial MMCs are considerably finer, 10 to 15 μm. Smaller particles may exhibit clustering, since surface forces are more significant. Consequently, the present results should be cautiously extrapolated to smaller particles.

The present work demonstrates that the settling behavior of high volume fractions of particles in liquid metal can be modeled reasonably well. This paves the way for computational studies of solidification of MMCs. During solidification, sedimentation will occur, which, in turn, will change local volume fraction of particles. The local volume fraction of particles determines the local thermal

conductivity, heat capacity, and density required for even the simplest of thermal models in which convection is ignored.

In reality, convection will have a major effect on heat transfer, which can be demonstrated with the following simple argument. The conductive heat flux in one dimension over a distance L with a temperature difference ΔT is

$$q = k\frac{\Delta T}{L} \quad [28]$$

The convective heat flux due to transport of a packet of fluid over the same ΔT with a velocity U is

$$q_c = \rho_L C_p \Delta T U \quad [29]$$

The ratio of these two fluxes is the Peclet number for heat transfer:

$$\mathrm{Pe} = \frac{UL}{\alpha} \quad [30]$$

Taking values of α for aluminum of 4×10^{-5} m^2/s, 2 mm/s for the velocity, and L as 0.1 m yields a Peclet number of 5, indicating that convection is quite significant. Consequently, thermal equations for the particulate and liquid phases, allowing for heat transfer between them, must be developed in an analogous manner to the momentum equations (Eqs. [5] and [6]). Furthermore, the effects of natural convection must be included in the modeling through the inclusion of the appropriate buoyancy terms. Work on the coupled thermal and convective flow is now underway.

Most of the modeling work performed on particle pushing by a solidification front has focused on the movement of single particles. The present work shows that the movement of a high-volume fraction particle phase is considerably more complicated. Indeed, the combined effects of convection and conduction must be properly addressed to determine how particle pushing actually operates.

VI. CONCLUSIONS

1. A novel four-point electrical resistance probe was developed to measure the *in situ* volume fraction of ceramic particles in liquid metal.
2. The technique was used to measure the rates at which high volume fractions (0.05 to 0.3) of 90-μm SiC particles settled in A356 aluminum alloy used for MMC fabrication.
3. A distinct clarification front was evident at low volume fractions. The front became slower and broadened at higher volume fractions.
4. A one-dimensional two-phase flow model for the solid and liquid phases was developed to model the sedimentation process. Surprisingly good agreement between the model and experimental results was obtained with an interphase drag function derived from the momentum balance equation, with the utilization of the Richardson-Zaki equation for particle settling in aqueous systems. Drag functions were also extracted from the experimental results.
5. There was little evidence of clustering of the particles during settling.

NOMENCLATURE

C_D	drag coefficient
C_p	specific heat (kJ kg^{-1} K^{-1})
d	diameter (μm)
F_D	drag force (N m^{-3})
g	gravitational acceleration (m s^{-2})
K	thermal conductivity (W m^{-1} K^{-1})
L	length (m)
P	pressure (N m^{-2})
q	conductive heat flux (W m^{-2})
T	temperature (K)
t	time (s)
U	velocity (m s^{-1})
U_0	Stokes velocity (m s^{-1})
x	spatial coordinate (m)

Greek Symbols

α	thermal diffusivity (m^2 s^{-1})
β	friction coefficient (kg m^{-3} s^{-1})
μ	viscosity (kg m^{-1} s^{-1})
ρ	density (kg m^{-3})
Θ	volume fraction
$\Theta(i,j)$	array of volume fractions; the indices i and j denote node and time, respectively

Subscripts

c	convective
L	liquid
p	particle
s	solids

ACKNOWLEDGMENTS

The authors wish to thank Mr. O. Kelly for his help with the experimental work. The financial support of the Ontario Centre for Materials Research and the material donations from ALCAN International and Norton Advanced Ceramics of Canada, Inc., are gratefully acknowledged.

REFERENCES

1. A.D. McLeod, C. Gabryel, D.J. Lloyd, and P. Morris: in *Processing of Ceramic and Metal Matrix Composites*, H. Mostaghaci, ed., CIM Conf. of Metallurgists, Aug. 20–24, 1989, Pergamon Press, New York, NY, pp. 228-35.
2. G.S. Hanumanth and G.A. Irons: in *Fabrication of Particulates Reinforced Metal Composites*, J. Masounave and F.G. Hamel, eds., ASM INTERNATIONAL, Metals Park, OH, 1990, pp. 41-46.
3. M. Mada and F. Ajersch: in *Metal and Ceramic Matrix Composites: Processing, Modelling and Mechanical Behaviour*, R.B. Bhagat, A.H. Clauer, P. Kumar, and A.M. Ritter, eds., TMS, Warrendale, PA, 1990, pp. 337-50.
4. R.B. Bird, W.E. Stewart, and E.L. Lightfoot: *Transport Phenomena*, John Wiley and Sons Inc., New York, NY, 1960, p. 60.
5. G.J. Kynch: *Trans. Faraday Soc.*, 1952, vol. 48, pp. 166-76.
6. F.M. Tiller: *AIChEJ*, 1981, vol. 27, pp. 823-29.

7. J.F. Richardson and W.N. Zaki: *Trans. Inst. Chem. Eng.*, 1954, vol. 32, pp. 35-53.
8. G.B. Wallis: *Proc. Symp. on Interactions between Fluids and Particles*, Institute of Chemical Engineers, London, 1962, vol. 9, pp. 9-16.
9. S. Lafreniere and G.A. Irons: *Int. Symp. on Production, Refining, Fabrication and Recycling of Light Metals*, Hamilton, ON, Canada, Aug. 1990, CIM, pp. 177-86.
10. D.C. Dixon: *AIChEJ.*, 1980, vol. 26, pp. 471-77.
11. Y.T. Shih, D. Gidaspow, and D.T. Wasan: *Powder Technol.*, 1987, vol. 50, pp. 201-15.
12. G. Hetsroni: *Handbook of Multiphase Systems*, McGraw-Hill, New York, NY, 1982.
13. D. Gidaspow: *Appl. Mech. Rev.*, 1986, vol. 39, pp. 1-22.
14. R.F. Sincovec and N.K. Madsen: *ACM Trans. Mathematical Software*, 1975, vol. 1, pp. 232-60.
15. A.C. Hindmarsh: in *Scientific Computing*, R.S. Stepleman, M. Carver, R. Peskin, W.F. Ames, and R. Vichnevetsky, eds., North-Holland, Amsterdam, 1983, pp. 55-64.